RSC Advances

PAPER

View Article Online
View Journal | View Issue

Cite this: *RSC Adv.*, 2016, **6**, 50688

Thermally stable ferrocene-α-cyanostilbenes as efficient materials for second order nonlinear optical polarizability†

Sugandha Dhoun,‡[a] Griet Depotter,‡[b] Sarbjeet Kaur,[a] Paramjit Kaur,*[a] Koen Clays[b] and Kamaljit Singh*[a]

Received 19th April 2016
Accepted 16th May 2016

DOI: 10.1039/c6ra10084h

www.rsc.org/advances

A set of new ferrocene-α-cyanostilbene (Fc-α-CNS) conjugated dyads was synthesized and their optical, nonlinear optical (NLO) and electrochemical properties were investigated. The second-order nonlinear polarizabilities were determined using hyper-Rayleigh scattering (HRS) with femtosecond pulsed laser light at 840 nm. The dyads exhibit structure-dependent NLO properties, which could be rationalized by correlating optical with electrochemical data. The dyad with the strongest (formyl) acceptor group in combination with the longer conjugation path between this acceptor and the Fc (ferrocene) donor, showed the largest static hyperpolarizability value, as compared to dyads with shorter conjugation and/or weaker acceptors. A partially symmetrical and longer triad showed the longest absorption wavelength, yet the smallest dipolar properties (dipole moment and first hyperpolarizability), are due to partial cancellation, in agreement with symmetry correlations.

Introduction

Nonlinear optical (NLO)[1–5] responsive materials are of great interest for applications related to photonics,[6,7] nanophotonics[8] and optoelectronics,[9–12] such as integrated optics, optical sensing, optical signal processing, optical computing, broad band optical communications, optical poling, optical limiting, *etc.* Standard materials frequently contain a donor–acceptor (D–A) combination intercepted by a conjugated bridge.[13–15] Amongst the various categories of compounds, the NLO response of ferrocene (Fc) based dyads, wherein a Fc donor (D) is linked to an appropriate acceptor (A) has been the subject of intensive investigations owing to many attractive features.[16–20] For example, electrochemical or chemical alteration of the oxidation state from +2 to +3 of the metal centre renders Fc a strong donor or acceptor, depending upon the oxidation state. This concept has lent practicability to the electrochemical redox switching[21–27] of the NLO response of the Fc D–A dyads. Fc generally possess low oxidation potential and is capable of a facile charge transfer (CT) to an acceptor to yield stable α-ferrocenyl carbocations.[17,28,29] Further, since the non-centrosymmetric D–A dyads are usually associated with high optical nonlinearities,[24,30–32] suitably functionalized push–pull dyads (D–π–A) in which electron donor Fc is connected through π-conjugating spacers to strong electron acceptors, have witnessed significant interest in their synthesis and properties. Interesting trends in the structure dependent electrochemical, optical and nonlinear optical properties have been reported.[31,33,34] Correlating the linear, electrochemical, theoretical calculations and hyper-Rayleigh scattering (HRS) experiments, we earlier[25] demonstrated that in contrast to the modulation of the acceptor strength, increasing the conjugation pathway (π-bridge) between Fc and the acceptor exerts a greater influence (red shift of the absorption band and smaller optical band gap) on the NLO response. Thus, the Fc based (D–π–A) compounds with shortest conjugation path depicted higher intrinsic hyperpolarizability compared to their longer conjugation counterparts. Additionally, owing to their reversible redox behaviour,[35–38] these chromophores recorded different hyperpolarizability values in each of the two (+2 and +3) redox states and a high on/off (β_{on}/β_{off}) ratio (switchability). Recently, we also reported that the ferrocene-diketopyrrolopyrrole[39] dyads exhibit higher nonlinear polarizability, β, which is modulated upon increasing the strength of acceptor as well as the length of intervening π-conjugation, although the effect of former is more pronounced.

In the family of D–A dyads, where α-cyanostilbene (α-CNS) is used as an acceptor are efficient luminophores and show photoactivity, tunable fluorescence,[40] and aggregation-induced enhanced emission (AIEE)[41–43] leading to potential applications in biological imaging,[44,45] optoelectronic devices such as organic field-effect transistors (OFETs),[46,47] organic light

[a]*Department of Chemistry, UGC Centre of Advance Study-II, Guru Nanak Dev University, Amritsar-143005, India. E-mail: kamaljit.chem@gndu.ac.in*

[b]*Department of Chemistry, University of Leuven, Celestijnenlaan 200D, B-3001 Leuven, Belgium. E-mail: koen.clays@fys.kuleuven.be*

† Electronic supplementary information (ESI) available. See DOI: 10.1039/c6ra10084h

‡ The first two authors contributed equally.

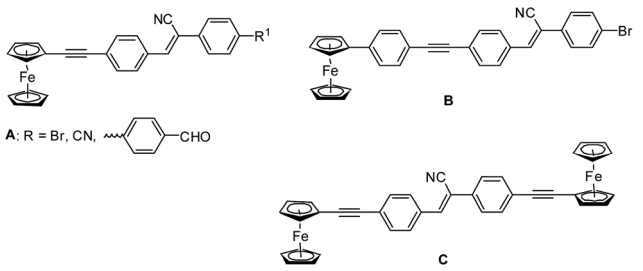

Fig. 1 Design strategies of Fc-α-CNS D–A (A and B) and D–A–D (C) chromophores.

emitting diodes (OLEDs)[48,49] and solar cells[49,50] *etc.* However, the NLO behaviour of Fc-α-CNS dyads has not been fully addressed. Taking into account, the flexibility in the structural diversification, thermal stability and unique photophysical properties of these π-conjugated luminophores, herein, we report the synthesis, linear optical and NLO properties of new chromophores having a Fc donor and an appropriately substituted α-CNS as an acceptor intercepted by a conjugated linker, representing D–A (dyad) and D–A–D (triad) designs. In the latter, the acceptor is flanked by two Fc units through a conjugated bridge.

In this work, new D–A or D–A–D type designs having a Fc donor and an appropriately substituted α-CNS acceptor, intercepted by a conjugated linker have been synthesized and the design principles are shown in Fig. 1. Their structure is determined by means of UV-visible absorption spectra, FTIR spectroscopy, mass spectrometry and ^{1}H and ^{13}C NMR spectral and microanalytical data. The NLO properties have been determined in dichloromethane (DCM) solution using hyper-Rayleigh scattering (HRS) technique using femtosecond pulsed 840 nm laser light. The linear optical data of the above chromophores has also been computed using density functional theory (DFT) calculations (Gaussian 09) and revealed a good correlation between the experimental results and the theoretically calculated data. Energies of the frontier molecular orbitals (FMOs) have been computed from time dependent DFT (TD-DFT) calculations and spectral resolution has been achieved by band fitting (OriginPro 8). Moreover, the structure–dipole moment relationship has also been deduced and the effect of the molecular design on the observed linear, electrochemical and NLO properties has been discussed.

Experimental section

Materials and reagents

All liquid reagents were dried/purified by using the recommended drying agents and/or distilled over 4 Å molecular sieves. Tetrahydrofuran (THF) and toluene were dried using sodium benzophenone ketyl while *N*,*N*-dimethylformamide (DMF) was distilled over CaH_2 and stored over 4 Å molecular sieves. Acetyl ferrocene[51] and bis(triphenylphosphine)dichloropalladium(II)[52] were prepared following the reported procedures. Ferrocene and 4-bromobenzaldehyde were purchased from Spectrochem and used as received. 4-Bromophenylacetonitrile, 4-formylphenylboronic acid, copper cyanide, copper(I) iodide and tetrakis(triphenylphosphine)palladium(0) were purchased from Sigma Aldrich and used as such. Ethynylferrocene **2**[39,53] and 4-(ethynylphenyl)ferrocene **3**[39,54] were prepared by the reported methods. All reported yields are isolated yields. Melting points were recorded in open capillaries and are uncorrected. For column chromatography, silica gel (60–120 mesh) was employed and eluted with ethyl acetate/hexane mixtures.

Instrumentation

UV-visible absorption recordings were carried out using HITACHI U-2910 Spectrophotometer. ^{1}H NMR and ^{13}C NMR spectra were recorded on Bruker Biospin Avance III HD at 500 MHz, in $CDCl_3$ containing tetramethylsilane (TMS) as internal standard. Data are reported as chemical shift in ppm (δ), integration, multiplicity (s = singlet, d = doublet, t = triplet, m = multiplet, br = broad) and coupling constant J (Hz). Infrared spectra were recorded on Perkin-Elmer FTIR-C92035 Fourier-transform infrared (FT-IR) spectrophotometer in range 400–4000 cm^{-1} as KBr pellets. Electrochemical measurements were made using CHI660D electrochemical workstation using three electrodes: platinum as working as well as counter electrode and Hg/Hg_2Cl_2 as reference electrode. The experiments were carried at 1×10^{-4} M solution of a compound in DCM using 2×10^{-2} M tetrabutylammoniumhexafluorophosphate as supporting electrolyte. The solutions were purged with dry nitrogen gas for 10 min and the working electrode as well as the reference electrode was cleaned after each reading. The experiments were carried out at scan rate of 100 mV s^{-1}. Thermogravimetric analyses (TGA) were recorded on TGA/DSC 1 STAR SYSTEM FROM METTLER TOLEDO in the temperature range of 0–800 °C at the heating rate of 10 °C min^{-1} under nitrogen atmosphere. Spectroelectrochemical studies were performed using Spectro-electrophotometer K-MAC SV2100-BF-0121. Femtosecond HRS measurements[55–60] were performed at 840 nm using a femtosecond pulsed Ti: sapphire laser. The pulse duration is 130 fs at a repetition rate of 80 MHz for an average power of 1.8 watt at 840 nm. This results in a peak power of 220 kW, in front of the waveplate/polarizer/lens train of optical elements before being focused in the sample. Crystal violet (C.I. Basic violet 3) in methanol was used as the reference, with a value of 434×10^{-30} esu at 840 nm corresponding to the octopolar β_{xxx} hyperpolarizability tensor component.

Computational details

Ab initio quantum mechanical calculations were performed using Gaussian 09 suite of programs.[61] Optimization of molecular geometries of **4–8** and related calculations were performed by DFT method using B3LYP functional group and 6-31G as the basis set. The first 20 excited states were calculated by using TD-DFT in gas phase as well in DCM as solvent using CPCM model. The molecular orbital contours were visualized using Gauss view 5.0.9.

Synthesis of dyads and intermediates

Synthesis of (*Z*)-2,3 bis-(4-bromophenyl)acrylonitrile 1. To a solution of 4-bromobenzaldehyde (2.0 g, 10.81 mmol) and 4-bromophenylacetonitrile (2.5 g, 12.75 mmol) in dry methanol (30 ml), a solution of sodium methoxide (1.5 ml, 25 wt%) was added, dropwise with vigorous stirring. Upon completion of the addition, the mixture turned cloudy and the suspension was stirred for another 2 h, at room temperature and subsequently cooled, which resulted in the precipitation of the product, which was filtered and recrystallized from ethanol to obtain analytically pure **1** as white solid (80%). Mp: 120–122 °C. IR (KBr) ν_{max}: 1363, 1400, 1492, 1586, 1904, 2220, 2855, 2925, 3048 cm^{-1}. ^1H NMR (500 MHz, $CDCl_3$, 25 °C) δ/ppm: 7.45 (s, 1H, –CH), 7.51–7.61 (m, 6H, Ar-H) and 7.75 (d, $J = 14$ Hz, 2H, Ar-H). ^{13}C NMR (125 MHz, $CDCl_3$, 25 °C) δ/ppm: 111.4, 117.3, 123.7, 125.2, 127.5, 130.7, 132.3, 133.1, 141.1. Anal. calculated for $C_{15}H_9NBr_2$: C, 49.62; H, 2.50; N, 3.86; found: C, 49.86; H, 2.89; N, 3.52.

General procedure for synthesis of 4, 8 and 7

A septum capped two-neck round bottom flask containing **1** (0.1 g, 0.2 mmol), CuI (0.003 g, 0.016 mmol), bis(triphenylphosphine)dichloropalladium(II) (0.015 g, 0.02 mmol) and cesium carbonate (0.448 g, 1.3 mmol) was flushed with dry nitrogen gas. Dry THF (10 ml) was added using hypodermic syringe at room temperature followed by evacuation and refilling with N_2 gas once again. A solution of **2** (0.057 g, 0.27 mmol) in anhydrous THF (5 ml) maintained under inert atmosphere was added dropwise to the reaction mixture at room temperature. Subsequently, the reaction mixture was heated to 85 °C for 4 h. After the completion of TLC (thin layer chromatography), the reaction mixture was extracted with ether (50 ml). The combined ether extract was washed with water (3 × 20 ml) and the organic layer dried over anhydrous sodium sulfate. The solvent was removed under reduced pressure to obtain crude mass, which was purified by column chromatography using 5 : 95 (ethyl acetate/hexane) as eluent to isolate analytically pure **4** (60%). Following the same procedure, using CuI (0.003 g, 0.016 mmol), bis(triphenylphosphine)dichloropalladium(II) (0.015 g, 0.02 mmol) and cesium carbonate (0.448 g, 1.3 mmol) and **2** (0.173 g, 0.82 mmol), **8** was obtained in 50% yield. Likewise, using **1** (0.1 g, 0.2 mmol), CuI (0.003 g, 0.016 mmol) and bis(triphenylphosphine)dichloropalladium(II) (0.015 g, 0.02 mmol) and **3** (0.15 g, 0.5 mmol), **7** was obtained in 62% yield. Further, in these reactions significant amounts of the corresponding diacetylene coproduct as a consequence of Glaser coupling reaction was also isolated.[62] The characteristic data of **4**, **7** and **8** is presented below.

(*Z*)-3-(4-Bromophenyl)-2-(4-(2-ferrocenylethynyl)phenyl) acrylonitrile 4. Orange solid. Mp 155–157 °C. IR (KBr): ν_{max} 1022, 1104, 1261, 1411, 1589, 2206, 2346, 2853, 2952, 2962 cm^{-1}. ^1H (500 MHz, $CDCl_3$, 25 °C): δ/ppm 4.26 (s, 5H, Fc), 4.29 (s, 2H, Fc), 4.54 (s, 2H, Fc), 7.48 (s, 1H, –CH), 7.54–7.64 (m, 6H, Ar-H) and 7.86 (d, $J = 10$ Hz, 2H, Ar-H). ^{13}C NMR (125 MHz, $CDCl_3$, 25 °C): δ/ppm 69.11, 69.19, 70.03, 70.06, 71.53, 71.61, 123.51, 125.83, 126.66, 127.46, 129.29, 130.67, 131.78, 131.96, 132.28, 133.47 and 141.67. Anal. calculated for $C_{27}H_{18}BrFeN$: C, 65.89; H, 3.69; N, 2.85; found: C, 65.96; H, 3.78; N, 2.82.

(*Z*)-3-(4-Bromophenyl)-2-(4-(2-(4-ferrocenylphenyl)ethynyl) phenyl)acrylonitrile 7. Orange solid. Mp 162–164 °C. IR (KBr): ν_{max} 1030, 1104, 1176, 1261, 1414, 1465, 1739, 2214, 2349, 2850, 2918 cm^{-1}. ^1H (500 MHz, $CDCl_3$, 25 °C): δ/ppm 4.05 (s, 5H, Fc), 4.37 (s, 2H, Fc), 4.68 (s, 2H, Fc) and 7.44–7.90 (m, 13H, –CH and Ar-H). ^{13}C NMR (125 MHz, $CDCl_3$, 25 °C): δ/ppm 69.08, 69.17, 70.03, 70.06, 71.53, 71.60, 125.80, 129.29, 131.76, 131.93, 132.58, 133.73 and 141.14. Anal. calculated for $C_{33}H_{22}BrFeN$: C, 69.75; H, 3.90; N, 2.46; found: C, 69.87; H, 3.83; N, 2.59.

(*Z*)-2,3-Bis(4-(2-ferrocenylethynyl)phenyl)acrylonitrile 8. Orange solid. Mp 177–178 °C. IR (KBr): ν_{max} 1019, 1104, 1261, 1383, 1410, 1599, 1638, 1741, 2202, 2366, 2922, 2959, 3095 cm^{-1}. ^1H (500 MHz, $CDCl_3$, 25 °C): δ/ppm 4.26 (s, 10H, Fc), 4.29 (s, 4H, Fc), 4.54 (s, 4H, Fc), 7.52–7.57 (m, 5H, –CH and Ar-H), 7.65 (d, $J = 10$ Hz, 2H, Ar-H) and 7.88 (d, $J = 10$ Hz, 2H, Ar-H). ^{13}C NMR (125 MHz, $CDCl_3$, 25 °C): δ/ppm 66.57, 69.48, 69.55, 69.75, 125.88, 127.50, 129.32, 130.71, 131.72, 131.79, 132.00, 132.16, 132.30, 132.51 and 141.55. Anal. calculated for $C_{39}H_{27}Fe_2N$: C, 75.39; H, 4.38; N, 2.25; found: C, 75.20; H, 4.53; N, 2.49.

Synthesis of (*Z*)-3-(4-formylphenyl)phenyl-2-(4-(2-ferrocenylethynyl)phenyl)acrylonitrile 6

A septum capped two-neck round bottom flask containing **4** (0.05 g, 0.1 mmol) dissolved in dry toluene (10 ml), was evacuated and charged with dry nitrogen gas and tetrakis(triphenylphosphine)palladium(0) (0.009 g, 0.008 mmol), potassium carbonate (2 M, 5 ml) and 4-formylphenylboronic acid (0.015 g, 0.1 mmol) were added in sequence. The reaction mixture was heated to 100 °C for 5 h. After completion of the reaction, solvent was removed under reduced pressure and compound was extracted with ether (2 × 25 ml). The combined ether extract was washed with water (3 × 20 ml) and the organic layer dried over anhydrous sodium sulfate. Removal of the solvent under reduced pressure furnished crude **6**, which was purified by column chromatography using 5 : 95 (ethyl acetate/hexane) as eluents to isolate analytically pure **6** (70%). Mp 158–160 °C IR (KBr): ν_{max} 1020, 1261, 1384, 1603, 1639, 2200, 2349, 2852, 2924 cm^{-1}. ^1H (500 MHz, $CDCl_3$, 25 °C): δ/ppm 4.27 (s, 5H, Fc), 4.29 (s, 2H, Fc), 4.54 (s, 2H, Fc), 7.57–8.03 (m, 13H, –CH and Ar-H) and 10.08 (s, 1H, –CHO). ^{13}C NMR (125 MHz, $CDCl_3$, 25 °C): δ/ppm 69.23, 70.09, 71.63, 125.86, 126.60, 127.62, 127.68, 128.00, 129.35, 130.01, 130.39, 131.78, 131.96, 132.49, 134.59, 135.60, 141.60 and 191.78. Anal. calculated for $C_{34}H_{23}FeNO$: C, 78.93; H, 4.48; N, 2.71; found: C, 78.72; H, 4.28; N, 2.92.

Synthesis of 4-((*Z*)-2-cyano-2-(4-(2-ferrocenylethynyl)phenyl) vinyl)benzonitrile 5

A solution of compound **4** in dry DMF (8 ml) was maintained under the atmosphere of dry nitrogen gas and copper(I) cyanide (0.418 g, 4.6 mmol) was added using a solid addition tube. The reaction mixture was heated for 24 h at 85 °C, after which, the solvent was removed under reduced pressure and compound was extracted with DCM (3 × 20 ml). The combined organic

extract was washed with water (3 × 20 ml) and the organic portion dried over anhydrous sodium sulfate. Removal of the solvent under reduced pressure yielded crude product, which was purified by column chromatography using 10 : 90 (ethyl acetate/hexane) as eluents to isolate analytically pure orange solid **5** (75%). Mp 172–174 °C IR (KBr): ν_{max} 1096, 1261, 1409, 1465, 1585, 2199, 2223, 2854, 2925, 2962 cm^{-1}. ^1H (500 MHz, $CDCl_3$, 25 °C): δ/ppm 4.27 (s, 5H, Fc), 4.30 (s, 2H, Fc), 4.54 (s, 2H, Fc) and 7.57–7.92 (m, 9H, –CH and Ar-H) ^{13}C NMR (125 MHz, $CDCl_3$, 25 °C): δ/ppm 59.37, 68.18, 68.28, 69.07, 70.56, 70.65, 84.47, 91.85, 108.60, 111.73, 113.04, 125.06, 125.49, 128.59, 128.63, 130.84, 131.02, 131.65, 131.84 and 142.91. Anal. calculated for $C_{28}H_{18}FeN_2$: C, 76.73; H, 4.14; N, 6.39; found: C, 76.82; H, 4.41; N, 6.52.

Results and discussion

Synthesis and characterization

Dyad (*Z*)-3-(4-bromophenyl)-2-(4-(2-ferrocenylethynyl)phenyl) acrylonitrile **4** was prepared (Scheme 1) in 60% yield through Sonogashira coupling reaction[63,64] of (*Z*)-2,3-bis-(4-bromophenyl)acrylonitrile **1** and ethynylferrocene **2** using bis (triphenylphosphine)dichloropalladium(II) and CuI as catalysts. A similar reaction of **1** with 4-(ethynylphenyl)ferrocene **3**, furnished (*Z*)-3-(4-bromophenyl)-2-(4-(2-(4-ferrocenylphenyl) ethynyl)phenyl) acrylonitrile **7** in 62% isolated yield. Increasing the stoichiometric amount of **2** to 0.5 mmol in reaction with **1** (0.2 mmol), led to the isolation of the triad (*Z*)-2,3-bis(4-(2-ferrocenylethynyl)phenyl)acrylonitrile **8** in 50% yield. Dyad **4** served as a common precursor for preparing the other two dyads **5** and **6**. Thus, heating **4** with cuprous cyanide at 80 °C led to the formation of 4-((*Z*)-2-cyano-2-(4-(2-ferrocenylethynyl)phenyl)vinyl) benzonitrile **5** in 75% yield (Scheme 1). Finally, Suzuki coupling[65] of **4** with 4-formylphenylboronic acid using Pd(0) in toluene provided (*Z*)-3-(4-formylphenyl)phenyl-2-(4-(2-ferrocenylethynyl)phenyl) acrylonitrile **6** in 70% isolated yield. All compounds were characterized by the correct spectroscopic and microanalytical data.

Thermogravimetric analysis

For a material to be used in electro-optic devices, it must possess high thermal stability to endure high processing temperatures (>200 °C). Thermal stability of all these chromophores was measured by thermogravimetric analysis (TGA) at a heating rate of 10 °C min^{-1} under nitrogen. TGA data of **4–8** attested thermal stability upto 300 °C (see ESI Fig. S1†). Thus, the good thermal stability of these chromophores makes them suitable candidates for practical device fabrication and heat-resistant materials.

UV-visible absorption characteristics

Dyads **4–7** and triad **8** show intense high energy (HE) and weak intensity low energy (LE) bands in the region of 352–364 nm and 460–476 nm, respectively (Fig. 2), which are characteristic of Fc based chromophores. Due to extensive mixing of the absorption bands, band fitting was applied to resolve the peaks using OriginPro 8 software (see ESI Fig. S2–S6†). Thus, the HE bands are assigned as intraligand $\pi \rightarrow \pi^*$ transitions while the LE bands are metal to ligand charge-transfer (MLCT) bands. The

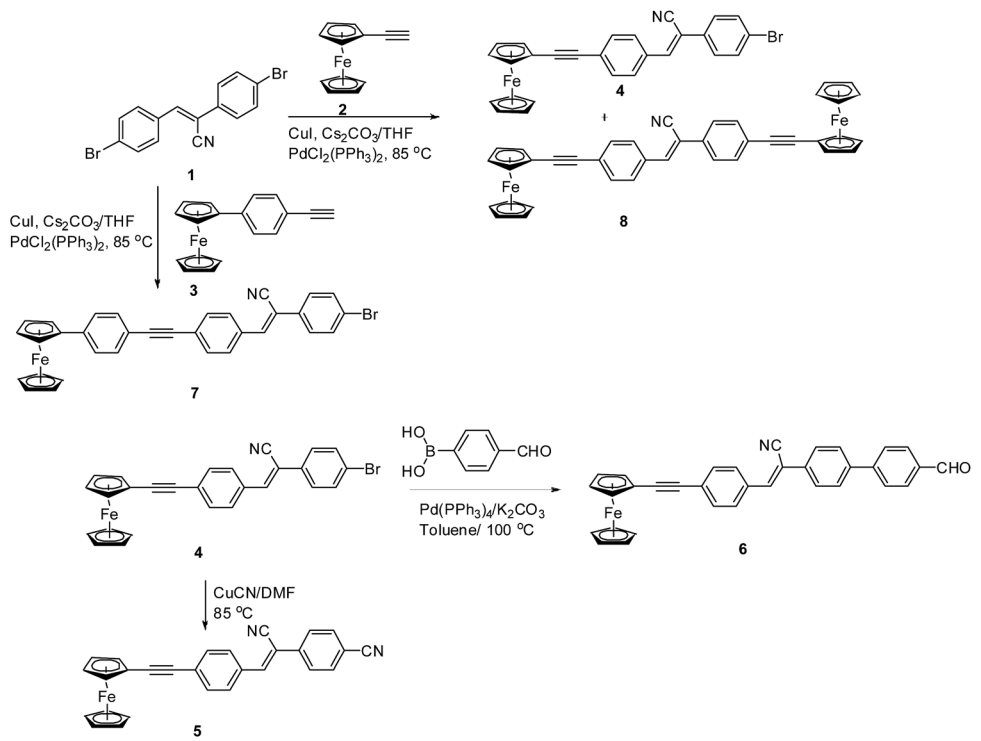

Scheme 1 Synthesis of ferrocene-α-cyanostilbene dyads, triad and their precursors.

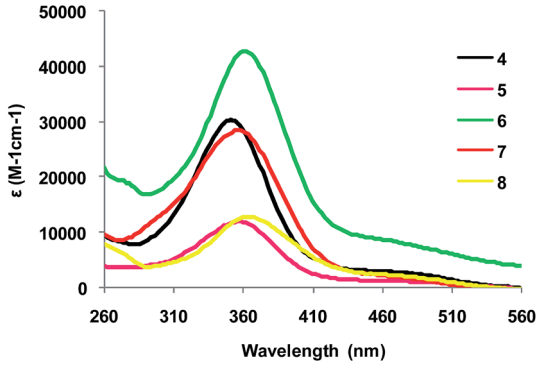

Fig. 2 Overlay of UV-visible absorption spectra of **4–8** in dichloromethane (1×10^{-5} M) at 293 K.

mixing of the HE and LE bands was also attested by the emission spectra (see ESI Fig. S7–S11 and Table S1†) of these chromophores as the emissive feature from both of these bands appear in the fluorescence spectra upon excitation at both the wavelengths corresponding to HE and LE bands. It has been observed that, sequential excitation of both HE and LE bands of these chromophores yielded emission covering the region of both HE and LE bands, however emission peaked at specific wavelengths (see ESI Fig. S7–S11†) in **4**, **6** and **8**, while in **5** and **7**, excitation at 474 nm and 356 nm, respectively, yielded a rather broad emission (see ESI Fig. S8a and S10†) suggesting mixing of HE and LE bands. The concentration dependence of absorption bands follows the Lambert–Beer law (see ESI Fig. S12†) as well as confirms their intramolecular nature. The assignment of $\pi \rightarrow \pi^*$ transition to the HE bands is made on the basis of the observation that upon changing the strength of the acceptor (compare **4** *vs.* **5**, **4** *vs.* **6**, **7** and **8** *etc.*, Table 1), the HE absorption band sees only a nominal red shift ($\Delta\lambda$ = 4–12 nm). The magnitude of this shift is however, smaller compared to similar Fc chromophores studied earlier.[25] On increasing the acceptor strength in **5**, compared to **4**, a red shift of 4 nm has been observed in the HE band. Likewise, a red shift of 10 nm is observed upon changing **4** to **6** due to the combined effect of increase in the acceptor strength and the intervening π-conjugation (insertion of phenyl ring). Further, upon increasing length of the π-conjugated bridge (compare **4** and **7**), the HE band shows red shift of 4 nm. However, the triad **8** with longest π-conjugated bridge shows largest red shift of 12 nm (**4** → **8**) for the HE band. Thus, it could be corroborated that HE transition is strongly dependent on the length of the conjugated chain, as changing **4** → **6** or **8** saw a red shift of 10 nm and 12 nm, respectively, confirming the $\pi \rightarrow \pi^*$ nature of these transitions. However, changing the acceptor strength showed only insignificant shift in the HE absorption band (**4** *vs.* **5**, $\Delta\lambda$ = 4 nm). Visualization of the electron density maps at isovalue 0.0004 (see ESI Fig. S13†) with the structural models superimposed, generated in Gauss view 5.09 revealed higher electron density on the α-CN function more than the formyl or the terminal cyano groups in **6** and **5**, respectively. The electron density on the bromo groups in **4** and **7** was minimal in accord with the observed trend in wavelengths of maximum absorption (HE bands) of these chromophores. The MLCT nature of the LE bands is ascertained from the fact that its position does not change (Table 1) significantly, upon changing the length as well as nature of the π-conjugated linker. This is corroborated by the positions of the bands deduced from the band fitted data (Table 1, see ESI Fig. S2–S6†) as owing to the extensive mixing of transitions in **4–8**, the experimental UV-visible absorption data is not in accordance with the established model for simpler Fc derived chromophores with only a single acceptor.[66] Further, during spectro-electrochemistry measurements on **4–8**, while the oscillator strength of the HE bands did not change significantly, the oscillator strength of the LE bands decreased almost completely upon electrochemical oxidation (see ESI Fig. S14–S17†) of Fc to ferrocenium, which served as additional proof of the LE band to be a MLCT band. The TD-DFT calculations on **4–8** further demonstrated contribution of appropriate HOMOs/LUMOs (see ESI Table S2†) to appropriate MLCT and/or d–d transitions. Further, the theoretically calculated wavelengths of absorptions of the HE bands as well as oscillator strengths of both LE and HE transitions corroborated the trend observed in the experimentally recorded UV-visible absorption spectra (see ESI Table S2†).

Table 1 HE and LE absorption bands, molar extinction coefficient and optical band gaps of **4–8**

	λ_{max}[a] (nm) [ε (M^{-1} cm^{-1})]; electronic transition(s)[b]		λ_{max}[c] (nm)	
	HE	LE	HE	LE
4	352 [30 300]; $\pi \rightarrow \pi^*$	476 [2700]; M → L	351	481
5	356 [12 000]; $\pi \rightarrow \pi^*$	474 [1200]; M → L, π–π^*	354	488
6	362 [42 600; $\pi \rightarrow \pi^*$	476 [8000]; M → L, d–d, π–π^*	360	481
7	356 [28 500]; $\pi \rightarrow \pi^*$	466 [2100]; M → L, d–d	351	477
8	364 [12 800]; $\pi \rightarrow \pi^*$	460 [2400]; M → L, d–d	364	486

[a] In DCM (10^{-5} M). [b] Assigned from TD-DFT deduced electron density isosurfaces of the maximum contributing HOMO and LUMO levels. [c] Band fitted data.

The absorption bands of chromophores **4–8** did not show solvent dependence or solvatochromism *i.e.* no significant red shift in the absorption bands was observed with increasing solvent polarity (see ESI Table S3†). However, as a consequence of photoexcitation, α-CNS are known[67,68] to exhibit twisted intramolecular charge transfer (TICT) effect owing to intramolecular rotation around the central bond. Since the TICT state produces a high dipole moment, these chromophores were expected to exhibit substantial second-order nonlinear optical properties. Chromophores **4–8** showed weak but broad fluorescence emission, covering almost the whole visible region, which might also have originated from the combined emission of the locally excited (HE) as well as TICT states.[69]

Electrochemistry

The chromophores **4–8** were studied by cyclic voltammetry to get a deeper insight into the ground state properties as well as mutual D–A electronic influence (see ESI Fig. S18–S22†).

Especially, it was interesting to know the variation of $E_{1/2}$ as well as highest occupied molecular orbital (HOMO), lowest unoccupied molecular orbital (LUMO) energies as a function of change in the molecular structures of **4–8**, which exhibited electrochemically reversible oxidation wave attributed to the Fe(III)/Fe(II) redox couple (Table 2). Upon changing Br in **4** with CN group in **5**, however did not show the expected anodic shift in the $E_{1/2}$ as well as stabilization of HOMO, which was expected owing to the influence of the stronger electron withdrawing CN group. Both $E_{1/2}$ as well as E_{pa} values were rather marginally lowered with this structural change. A comparison of the positions of the HE bands of the pairs of chromophores: **4**/**6** and **5**/**6** suggested a minor red shift of 10 and 6 nm, respectively. This was also reflected in nominal but favourable trend in $E_{1/2}$ ($\Delta E_{1/2}$: 0.0315 and 0.0045 V, respectively) as well as E_{pa} values (ΔE_{pa}: 0.049 and 0.011 V, respectively) recorded by the comparable pairs of **4**/**6** and **5**/**6**, respectively. Thus, the cathodic shift in the $E_{1/2}$ reflected increased electron density at the Fc donor, which resulted in both, the rise in HOMO energies (Table 3) as well as facile oxidation of Fc to ferrocenium species as compared to **4**. This marginal anodic shift of **8** ($E_{1/2} = 0.7865$ V) as compared to **4** ($E_{1/2} = 0.7715$ V) indicated marginally enhanced electronic communication in the D–A–D **8** compared to D–A **4**. This could be attributed to marginally stabilised HOMO in **8** (Table 3) as compared to **4**. On comparing **4** and **7**, as the π-conjugation increases, energy of HOMO (Table 3) of **7** increases along with the corresponding decrease in $E_{1/2}$ value ($\Delta E_{1/2}$: 0.0575 V) as well as E_{pa} value (ΔE_{pa}: 0.064 V).

Theoretical modelling

The series of chromophores **4–8** were studied theoretically to visualize the effect of donor and acceptor strength as well as the length and nature of the π-bridge, on the linear optical, electrochemical properties and the dipole moment. In order to rationalize the experimental absorption spectral data, TD-DFT calculations in both solvent and gas phase were carried out (see ESI Tables S4 and S5†). The calculated energies showed good correlation with the corresponding values deduced from CV and UV-visible absorption data (Table 3). Energies of the sets of HOMO and LUMO levels of **4–8** are listed in Table S4† (DCM phase) and Table S5† (gas phase). The plot of the frontier molecular orbital (FMO) energies of the chromophores (Fig. 3 and see ESI Fig. S23†) shows interesting correlations of the electronic absorption properties of the chromophores. Replacing Br in **4** with CN in **5**, the stabilization of the LUMO energy levels is in accord with the experimentally observed red shift in the absorption band, indicating increased strength of the acceptor in the latter. Similarly, with increasing the π-bridge conjugation length (compare **4** *vs.* **6**; **5** *vs.* **6**; **4** *vs.* **7** and **4** *vs.* **8**), while the energies of HOMO in all except **8** increased, the LUMO energies showed a decrease, which is also in agreement with the experimental optical data (Table 3), and corresponded to the observed decrease in optical band gap for these comparable set of chromophores. Thus, the effect of change in π-bridge conjugation length (**4** *vs.* **8**, for instance) on the HOMO–LUMO energy gap is more pronounced than the change in acceptor strength (**4** *vs.* **5**). Further, the electron density contours of principal orbitals involved in the main transitions plotted in (see ESI Fig. S24 and S25†), allowed accurate assignment of the experimentally observed bands. The HOMO is mainly located (see ESI Fig. S24 and S25†) on the Fc unit with significant contribution from the acetylene link and the adjoining phenyl ring, which constitute parts of the central π-bridge, while the LUMO is largely located on the acceptor, with additional contribution from the π-bridge. In agreement with this observation, the HE and LE bands in **4–8** were assigned appropriate transitions (Table 1). The π → π* HE band with highest oscillator strength for **4–7** corresponds to H-2 → LUMO and for **8** it is HOMO → LUMO (see ESI Table S2†). Further, in these chromophores, while the HE transition has main contribution from HOMO → LUMO or H-2 → LUMO, the LE bands have identical contribution from two or three transitions (see ESI Table S2†). Further, the β values are also in good agreement with change in the dipole moments (μ) of these chromophores (Table 3) as calculated from the theoretical calculations.

Table 2 Electrochemical data of **4–8** in DCM

	E_{pa} (V)	E_{pc} (V)	$E_{1/2}{}^{a}$ (V)	$i_{pa} \times 10^{-6b}$ (A)	$i_{pc} \times 10^{-6b}$ (A)
4	0.828	0.715	0.7715	−1.532	1.215
5	0.790	0.699	0.7445	−0.5723	0.3909
6	0.779	0.701	0.7400	−0.3617	0.2846
7	0.764	0.664	0.7140	−0.8934	0.7498
8	0.837	0.736	0.7865	−0.9542	0.6023

[a] Half-wave potential, $E_{1/2} = (E_{pc} + E_{pa})/2$, where E_{pc} and E_{pa} correspond to the cathodic and anodic peak potentials, respectively; $\Delta E_p = 80$–120 mV [$i_{pc}/i_{pa} \sim 1$] and a scan rate of 100 mV s^{-1}. [b] Amplitudes of the anodic and cathodic peaks.

Quadratic hyperpolarizabilities

The first hyperpolarizability, β, of the chromophores **4–8** was measured in DCM, using femtosecond hyper-Rayleigh scattering (HRS) method at 840 nm (Table 4). Crystal violet solution in methanol was used as reference. All compounds are stable under laser light as checked by recording UV-visible absorption spectra of the solutions before and after the HRS measurements. First hyperpolarizability, $\beta = 434 \times 10^{-30}$ esu was recorded at 840 nm for the octopolar β_{xxx} hyperpolarizability tensor component of the reference. Further, the LE MLCT bands are found to be in close proximity with the second harmonic generation wavelength (420 nm, Table 1), resulting in the resonance enhancement of the β values. Thus, the β values have been corrected for the resonance enhancement, $\beta_{HRS,0}$, using two-level model and are shown in Table 4. It is important to note that the two-level model provides an approximate measure of resonance enhancement as it is not fully applicable to the systems with multiple electronic transitions contributing to the absorption bands.

Among the series of the chromophores studied, **4**, with shortest π-conjugation bridge as well as weak acceptor showed the smaller $\beta_{HRS,0}$ (21×10^{-30} esu) as compared to **5** ($\beta_{HRS,0} = 27$

Table 3 Comparison of experimental (CV/UV-vis) and the calculated (TD-DFT) HOMO–LUMO energy data and dipole moments of **4–8**

	Experimental data			Calculated (TD-DFT) data (gas phase/DCM)[d]			
Compound	E_{HOMO}[a] (eV)	$E_g^{optical}$[b] (eV)	E_{LUMO}[c] (eV)	E_{HOMO} (eV)	E_{LUMO} (eV)	ΔE (eV)	μ (D)
4	−5.085	3.076	−2.009	−5.48146/−5.46758	−2.40031/−2.43786	3.08115/3.02972	5.2214/6.4070
5	−5.070	3.032	−2.038	−5.57724/−5.49370	−2.67324/−2.62100	2.90400/2.87270	8.0289/9.3951
6	−5.060	2.968	−2.092	−5.48717/−5.46268	−2.49338/−2.50753	2.99379/2.95515	7.2898/8.8644
7	−5.045	2.989	−2.056	−5.37289/−5.36765	−2.46399/−2.50181	2.9089/2.86584	5.4702/6.6195
8	−5.115	2.907	−2.208	−5.29642/−5.37180	−2.31160/−2.44031	2.98482/2.93149	4.0212/5.2736

[a] Calculated as $E_{HOMO} = -e[E_{ox}^{onset} + 4.4]$. [b] Calculated as $E_g^{optical} = 1240/\lambda_{onset}$. [c] Calculated as $E_{LUMO} = E_g^{optical} + E_{HOMO}$. [d] B3LYP/6-31G level.

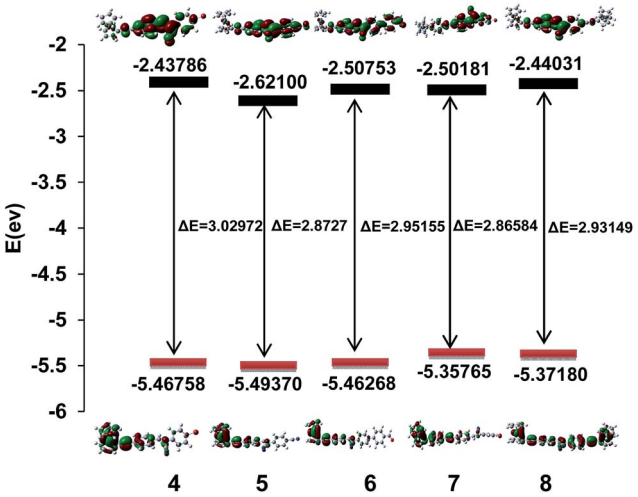

Fig. 3 Comparison of energies and energy gap (ΔE) of the FMOs (HOMO and LUMO) of **4–8** (TD-DFT at B3LYP/6-31G basis set in DCM phase).

Table 4 Quadratic nonlinear optical parameters of **4–8**

Compound	β_{HRS}[a] (10^{-30} esu)	$\beta_{HRS,0}$[b] (10^{-30} esu)
4	110 ± 10	21
5	146 ± 6	27
6	183 ± 8	35
7	182 ± 8	29
8	124 ± 7	17

[a] Second-order nonlinear polarizability, β_{HRS} recorded at 840 nm in DCM. [b] Second-order nonlinear polarizability, $\beta_{HRS,0}$ corrected for resonance enhancement.

$\times 10^{-30}$ esu). This could be attributed to the replacement of Br with CN, reflecting marginally greater acceptor strength of the latter. This increase in $\beta_{HRS,0}$ value (**4** → **5**) is further supported by the two-level model,[70,71] as both dipole moment (Table 3) and oscillator strength (*f*, see ESI Table S2†) increases on increasing the acceptor strength in latter as well as the decrease in the optical band gap is observed in the latter (Table 3). Chromophores **6** and **7** recorded higher $\beta_{HRS,0}$ values (35×10^{-30} esu and 29×10^{-30} esu, respectively) as compared to **4** (Table 4). This increase in $\beta_{HRS,0}$ value for **6** and **7**, compared to **4**, could be attributed to the combined effect of the increase in the length of the π-conjugation bridge as well as acceptor strength in the former and the influence of the π-conjugation bridge in the latter. Additionally, the chromophores **6** and **7** exhibited larger dipole moments (Table 3) and oscillator strength (*f*, see ESI Table S2†) as well as small band gaps (Table 3), as compared to **4**. Also, the chromophore **6** shows slightly large $\beta_{HRS,0}$ value as compared to **7**, owing to the combined effect of the larger dipole moment and small band gap (Table 3) in the former, however, the latter has greater oscillator strength (*f*, Table S2, ESI†) as well as larger band gap compared to **6**. Further, chromophore **6** also showed larger $\beta_{HRS,0}$ value compared to **5**, although the acceptor strength of latter is more as inferred from the dipole moments (**5** > **6**, Table 3). This could be attributed to the increased π-conjugation in **6** as well as the more availability of p-orbitals to participate in the charge transfer in formyl group than in nitrile group, resulting in increased β value of **6**. Also, chromophore **6** showed higher oscillator strength (*f*, see ESI Table S2†) and lower band gap (Table 3), resulting in the increased charge transfer and hence, increased $\beta_{HRS,0}$ value as compared to **5**. This was already inferred from the observed red shift of the HE bands (Table 1) in the optical data as well as the observed trend is in good agreement with the theoretical data. Consistent with the increase in the π-bridge length, a higher β values for the disubstituted chromophore **8** would be expected. However, it recorded smallest $\beta_{HRS,0}$ value of 17×10^{-30} esu, which implied a partial cancellation of charge transfer owing to the fact that the central acceptor unit is flanked by two Fc donors. As compared to **4**, chromophore **8** shows smaller $\beta_{HRS,0}$ value, due to lesser larger dipole moment (Table 3) and oscillator strength (*f*, see ESI Table S2†).

When comparing these hyperpolarizability values with the values for related chromophores, it is important to appreciate the combination of the ferrocene-derived properties with the α-CNS derived properties. α-CNS have not been thoroughly investigated for their second-order nonlinear optical properties. There is one report[72] with emphasis on the macroscopic nonlinearity of crystals, still reporting molecular hyperpolarizability values up to 74 $\times 10^{-30}$ esu at 1064 nm for the strong dimethylamino donor group. Our values with the redox-switchable Fc donor compare very favourably with these values. However, when comparing first hyperpolarizability values of Fc-donor based chromophores, with longer conjugation paths and much stronger acceptor moieties, based on tricyano-acceptors, larger hyperpolarizabilities have

been reported,[73] but with the concomitant compromise in transparency (absorption up to the NIR) and inefficiency (reduced nonlinearity per number of polarizable electrons). It has been shown that the Fc derivatives with the shorter conjugation path and the CHO and CN (monocyano) acceptor outperform the longer chromophores with tricyano-acceptors in terms of their intrinsic hyperpolarizability.[25]

Conclusions

Thus, the new Fc based chromophores show significant intrinsic hyperpolarizability. Correlating the UV-visible absorption, electrochemical, theoretical calculations and hyper-Rayleigh scattering experiments carried out for the chromophores, it was established that varying the conjugation path and/or acceptor strength would tune the non-linear optical properties. On increasing the π-bridge length, a greater red shift of the absorption bands and smaller HOMO–LUMO gaps are observed as compared to the ones observed in the case of changing the acceptor strength. Thus, these chromophores could be considered as promising candidates for electro-optic devices on the basis of the observed first hyperpolarizability as well as high thermal stability (upto 300 °C). It could also be expected that these chromophores could exhibit even better second-order nonlinearities by appending even stronger acceptors such as nitro, dicyanovinyl groups *etc.*

Acknowledgements

We are thankful to SERB-DST, New Delhi for the project SB/S1/OC-45/2013 as well as UPE fellowship for SD and CSIR, New Delhi for research fellowship to SK.

Notes and references

1 N. J. Long, *Angew. Chem., Int. Ed. Engl.*, 1995, **34**, 21–38.
2 D. R. Kanis, M. A. Ratner and T. J. Marks, Quantum Chemical Aspects, *Chem. Rev.*, 1994, **94**, 195–242.
3 S. R. Marder, B. Kippelen, A. K.-Y. Jen and N. Peyghambarian, *Nature*, 1997, **388**, 845–851.
4 I. R. Whittall, A. M. McDonagh, M. G. Humphrey and M. Samoc, *Adv. Organomet. Chem.*, 1998, **42**, 291–362.
5 K. A. Green, M. P. Cifuentes, M. Samoc and M. G. Humphrey, *Coord. Chem. Rev.*, 2011, **255**, 2025–2038.
6 P. N. Prasad and D. J. Williams, *Nonlinear Optical Effects in Molecules and Polymers*, Wiley, New York, 1991.
7 P. N. Prasad, *Nonlinear Optical Properties of Organic Materials*, Plenum, New York, 1991.
8 P. N. Prasad, *Nanophotonics*, Wiley, New York, 2004.
9 R. W. Boyd, *Nonlinear Optics*, Academic Press, New York, 1992.
10 Y. Shirota, *J. Mater. Chem.*, 2000, **10**, 1–25.
11 K. Clays and B. Coe, *Chem. Mater.*, 2003, **15**, 642–648.
12 M. G. Kuzyk, *J. Mater. Chem.*, 2009, **19**, 7444–7465.
13 S. R. Marder, D. N. Beratan and L.-T. Cheng, *Science*, 1991, **252**, 103–106.
14 M. Lamrani, R. Hamasaki, M. Mitsuishi, T. Miyashitab and Y. Yamamoto, *Chem. Commun.*, 2000, 1595–1596.
15 C. E. Powell and M. G. Humphrey, *Coord. Chem. Rev.*, 2004, **248**, 725–756.
16 S. Barlow and S. R. Marder, *Chem. Commun.*, 2001, 1555–1562.
17 P. Debroy and S. Roy, *Coord. Chem. Rev.*, 2007, **251**, 203–221.
18 R. Horikoshi and T. Mochida, *Eur. J. Inorg. Chem.*, 2010, 5355–5371.
19 R. D. A. Hudson, I. Asselberghs, K. Clays, L. P. Cuffe, J. F. Gallagher, A. R. Manning, A. Persoons and K. Wostyn, *J. Organomet. Chem.*, 2001, **637–639**, 435–444.
20 B. J. Coe, S. P. Foxon, M. Helliwell, D. Rusanova, B. S. Brunschwig, K. Clays, G. Depotter, M. Nyk, M. Samoc, D. Wawrzynczyk, J. Garin and J. Orduna, *Chem.–Eur. J.*, 2013, **19**, 6613–6629.
21 T. Weyland, I. Ledoux, S. Brasselet, J. Zyss and C. Lapinte, *Organometallics*, 2000, **19**, 5235–5237.
22 C. Sporer, I. Ratera, D. Ruiz-Molina, Y. Zhao, J. Vidal-Gancedo, K. Wurst, P. Jaitner, K. Clays, A. Persoons, C. Rovira and J. A. Veciana, *Angew. Chem., Int. Ed.*, 2004, **43**, 5266–5268.
23 M. Samoc, N. Gauthier, M. P. Cifuentes, F. Paul, C. Lapinte and M. G. Humphrey, *Angew. Chem., Int. Ed.*, 2006, **45**, 7376–7379.
24 B. J. Coe, *Acc. Chem. Res.*, 2006, **39**, 383–393.
25 P. Kaur, M. Kaur, G. Depotter, S. Van Cleuvenbergen, I. Asselberghs, K. Clays and K. Singh, *J. Mater. Chem.*, 2012, **22**, 10597–10608.
26 W.-Y. Wang, N.-N. Ma, S.-L. Sun and Y.-Q. Qiu, *Phys. Chem. Chem. Phys.*, 2014, **16**, 4900–4910.
27 B. J. Coe, S. P. Foxon, R. A. Pilkington, S. Sanchez, D. Whittaker, K. Clays, G. Depotter and B. S. Brunschwig, *Organometallics*, 2015, **34**, 1701–1715.
28 M. D. Ward, *Chem. Soc. Rev.*, 1995, **24**, 121–134.
29 T. Kuwana, D. E. Bublitz and G. L. K. Hoh, *J. Am. Chem. Soc.*, 1960, **82**, 5811–5817.
30 T. Verbiest, S. Houbrechts, M. Kauranen, K. Clays and A. Persoons, *J. Mater. Chem.*, 1997, **7**, 2175–2189.
31 S. Di Bella, *Chem. Soc. Rev.*, 2001, **30**, 355–366.
32 Y. Liao, S. Bhattacharjee, K. A. Firestone, B. E. Eichinger, R. Paranji, C. A. Anderson, B. H. Robinson, P. J. Reid and L. R. Dalton, *J. Am. Chem. Soc.*, 2006, **128**, 6847–6853.
33 N. Tsuboya, M. Lamrani, R. Hamasaki, M. Ito, M. Mitsuishi, T. Miyashita and Y. Yamamoto, *J. Mater. Chem.*, 2002, **12**, 2701–2705.
34 N. Tsuboya, R. Hamasaki, M. Ito, M. Mitsuishi, T. Miyashitab and Y. Yamamoto, *J. Mater. Chem.*, 2003, **13**, 511–513.
35 M. Malaun, Z. R. Reeves, R. L. Paul, J. C. Jeffery, J. A. McCleverty, M. D. Ward, I. Asselberghs, K. Clays and A. Persoons, *Chem. Commun.*, 2001, 49–50.
36 M. Malaun, R. Kowallick, A. M. McDonagh, A. M. Marcaccio, R. L. Paul, I. Asselberghs, K. Clays, A. Persoons, B. Bildstein, C. Fiorini, J.-M. Nunzi, M. D. Ward and J. A. McCleverty, *J. Chem. Soc., Dalton Trans.*, 2001, **2001**, 3025–3038.

37 I. Asselberghs, K. Clays, A. Persoons, A. M. McDonagh, M. D. Ward and J. A. McCleverty, *Chem. Phys. Lett.*, 2003, **368**, 408–411.
38 B. J. Coe, J. Fielden, S. P. Foxon, I. Asselberghs, K. Clays, S. V. Cleuvenbergen and B. S. Brunschwig, *Organometallics*, 2011, **30**, 5731–5743.
39 S. Kaur, S. Dhoun, G. Depotter, P. Kaur, K. Clays and K. Singh, *RSC Adv.*, 2015, **5**, 84643–84656.
40 Y. Zhang, J. Sun, X. Lv, M. Ouyang, F. Cao, G. Pan, L. Pan, G. Fan, W. Yu, C. He, S. Zheng, F. Zhang, W. Wanga and C. Zhang, *CrystEngComm*, 2013, **15**, 8998–9002.
41 B.-K. An, J. Gierschner and S. Y. Park, *Acc. Chem. Res.*, 2012, **45**, 544–554.
42 B.-K. An, S.-K. Kwon, S.-D. Jung and S. Y. Park, *J. Am. Chem. Soc.*, 2002, **124**, 14410–14415.
43 J. Gierschner and S. Y. Park, *J. Mater. Chem. C*, 2013, **1**, 5818–5832.
44 C.-K. Lim, S. Kim, I. C. Kwon, C.-H. Ahn and S. Y. Park, *Chem. Mater.*, 2009, **21**, 5819–5825.
45 X. Zhang, X. Zhang, B. Yang, Y. Yang and Y. Wei, *Polym. Chem.*, 2014, **5**, 5885–5889.
46 J. A. Mikroyannidis, A. N. Kabanakis, S. S. Sharma and G. D. Sharma, *Adv. Funct. Mater.*, 2011, **21**, 746–755.
47 S. W. Yun, J. H. Kim, S. Shin, H. Yang, B. K. An, L. Yang and S. Y. Park, *Adv. Mater.*, 2012, **24**, 911–915.
48 X. Li, Y. Xu, F. Li and Y. Ma, *Org. Electron.*, 2012, **13**, 762–766.
49 S. K. Park, S. Varghese, J. H. Kim, S. J. Yoon, O. K. Kwon, B.-K. An, J. Gierschner and S. Y. Park, *J. Am. Chem. Soc.*, 2013, **135**, 4757–4764.
50 W. Jia, P. Yang, J. Li, Z. Yin, L. Kong, H. Lu, Z. Ge, Y. Wu, X. Hao and J. Yang, *Polym. Chem.*, 2014, **5**, 2282–2292.
51 M. M. Hale, Creative Commons Attribution License (CC-BY 2.0).
52 A. M. McDonagh, N. T. Lucas, M. P. Cifuentes, M. G. Humphrey, S. Houbrechts and A. Persoons, *J. Organomet. Chem.*, 2000, **605**, 184–192.
53 J. Polin and H. Schottenberger, *Org. Synth.*, 1996, **73**, 262.
54 B. J. Coe, C. J. Jones and J. A. McCleverty, *J. Organomet. Chem.*, 1994, **464**, 225–232.
55 K. Clays and A. Persoons, *Phys. Rev. Lett.*, 1991, **66**, 2980–2983.
56 K. Clays and A. Persoons, *Rev. Sci. Instrum.*, 1992, **63**, 3285–3289.
57 K. Clays, A. Persoons and L. De Maeyer, *Adv. Chem. Phys.*, 1994, **85**, 455–498.
58 K. Clays and A. Persoons, *Rev. Sci. Instrum.*, 1994, **65**, 2190–2194.
59 G. Olbrechts, R. Strobbe, K. Clays and A. Persoons, *Rev. Sci. Instrum.*, 1998, **69**, 2233.
60 G. Olbrechts, K. Wostyn, K. Clays and A. Persoons, *Opt. Lett.*, 1999, **24**, 403–405.
61 M. J. Frisch, *et al.*, *Gaussian 09, Revision B.01*, Gaussian, Inc., Wallingford, CT, 2010, For complete reference see ESI.†
62 K. Balaraman and V. Kesavan, *Synthesis*, 2010, **20**, 3461–3466.
63 R. Chinchill and C. Najera, *Chem. Rev.*, 2007, **107**, 874–922.
64 R. Chinchilla and C. Najera, *Chem. Soc. Rev.*, 2011, **40**, 5084–5121.
65 N. Miyaura and A. Suzuki, *Chem. Rev.*, 1995, **95**, 2457–2483.
66 S. Barlow, H. E. Bunting, C. Ringham, J. C. Green, G. U. Bublitz, S. G. Boxer, J. W. Perry and S. R. Marder, *J. Am. Chem. Soc.*, 1999, **121**, 3715–3723.
67 L. Zhu and Y. Zhao, *J. Mater. Chem. C*, 2013, **1**, 1059–1065.
68 V. Palakollu and S. Kanvah, *New J. Chem.*, 2014, **38**, 5736–5746.
69 E. Gilabert, R. Lapouyade and C. Rulliere, *Chem. Phys. Lett.*, 1988, **145**, 262–268.
70 J. L. Oudar and D. S. Chemla, *J. Chem. Phys.*, 1977, **66**, 2664–2668.
71 J. L. Oudar, *J. Chem. Phys.*, 1977, **67**, 446–457.
72 H. Arai, Y. Higashigaki, M. Goto and S. Yano, *Jpn. J. Appl. Phys.*, 1994, **33**, 5755–5758.
73 Y. Liao, B. E. Eichinger, K. A. Firestone, M. Haller, J. Luo, W. Kaminsky, J. B. Benedict, P. J. Reid, A. K.-Y. Jen, L. R. Dalton and B. H. Robinson, *J. Am. Chem. Soc.*, 2005, **127**, 2758–2766.

